CrossMark

ORIGINAL PAPER

Electro-optical performance of inorganic monolithic electrochromic device with a pulsed DC sputtered Li_xMg_yN ion conductor

Yu Xiao[1] · Guobo Dong[1] · Qingjiao Huang[1] · Qirong Liu[1] · Junji Guo[1] · Jiang Liu[2] · Junying Zhang[1] · Xungang Diao[1]

Abstract Lithium magnesium nitride (Li_xMg_yN) thin films were deposited by pulsed DC reactive magnetron sputtering from a LiMg alloy target in the mixture gas of Ar and N_2. The as-prepared Li_xMg_yN films were amorphous. A monolithic inorganic electrochromic device (ECD) based on WO_3/NiO complementary structure was fabricated using the Li_xMg_yN as the ion conductor layer. The addition of a 150-nm thick Si_3N_4 buffer layer between Li_xMg_yN and NiO made coloration and bleaching reversible and stable. Electrochemical and optical characterizations were conducted to evaluate the performance of the ECD. Electro-optical data were recorded for both 1000 chronoamperometric cycles and 1000 voltammetric cycles. Activation and degradation of the electro-optical properties of the ECD were observed.

Keywords Monolithic electrochromic device · Smart windows · Lithium magnesium nitride · Electro-optical performance

Introduction

Electrochromic materials are capable of changing their optical properties persistently and reversibly by an applied voltage [1, 2]. They have drawn considerable attention over the last decades due to their potential applications, such as smart windows, information display, rearview mirrors, and variable-emittance thermal radiators [3–9]. For practical use, the electrochromic materials must be integrated into an electrochromic device (ECD). The most extensively investigated application of ECD is for architectural windows (smart windows), which provide a viable option for dynamic control of visible light and solar energy leading to life comfort and energy saving.

There are three fundamental components of the multilayer structure of an ECD, which are transparent conducting electrodes, electrochromic active layers, and an ion conductor. In_2O_3:Sn (ITO), SnO_2:F (FTO), and ZnO:Al (AZO) are known as the most commonly used transparent conductors. Among the inorganic electrochromic materials, thin films of tungsten oxide and nickel oxide are the most widely studied due to their high coloration efficiency, large dynamic range, and good cyclic reversibility [10–14]. Moreover, combining them makes it possible to modulate the overall optical transmittance and create a more neutral color device.

In the case of the smart windows, there are several advantages of employing an inorganic electrolyte. And among these are: (1) using inorganic electrolytes makes it possible for continuous, large area, in-line manufacturing processes (especially reactive sputtering and related physical deposition techniques), (2) monolithic structures with inorganic electrolytes can avoid bubble formation, potential liquid leak, and sealing problems during manufacture, (3) the stability and durability of inorganic films are expected to be high, especially with respect to exposure to a wide range of temperatures and ultraviolet radiation conditions. Much research has been published regarding the inorganic all-solid-state ECD. Table 1 summarizes the reported performance of inorganic monolithic electrochromic devices using different ion conductors. Many researchers have employed Ta_2O_5 thin film as the ion conductor [14–16, 24]. However, it generally takes a second procedure to inject ions

✉ Xungang Diao
diaoxg@buaa.edu.cn

[1] Electrochromism Center, School of Physics and Nuclear Energy Engineering, Beihang University, Beijing 100191, People's Republic of China

[2] Jiangsu Fanhua Glass Co., Ltd., Hai'an, Nantong, Jiangsu Province, People's Republic of China

Springer

Table 1 Reported performance of inorganic monolithic electrochromic devices

Device configuration	Colored/bleached potentials (V)	T (%)	t_{sw} (s)	Switching cycles	Ref.
H$^+$ based ECD					
G/ITO/NiO/Ta$_2$O$_5$/WO$_3$/ITO	+ 1.6/− 1.0	15–78	60	2×10^4	[15]
G/ITO/NiO/Ta$_2$O$_5$/WO$_3$/ITO	+ 1.5/− 1.5	18–73	–	10^5	[16]
G/ITO/NiV$_x$O$_y$H$_z$/ZrO$_2$/a-WO$_3$/grid Al	− 4/+ 5	15–50	> 600	–	[17]
G/ITO/WO$_3$/Ta$_2$O$_5$/NiO$_x$/Au	+ 2/− 2	3–58	6	–	[14]
G/ITO/NiO/ZrO$_2$/WO$_3$/ITO	+ 5/− 5	3–59	120	–	[18]
Li$^+$ based ECD					
G/ITO/WO$_3$/LiNbO$_3$/LiCoO$_2$/ITO	+ 3/− 3	12–65	–	1.8×10^4	[19]
G/ITO/Li$_x$V$_2$O$_5$/LiBO$_2$/WO$_3$/ITO	–	13–65	–	2×10^3	[20]
G/ITO/Li$_z$Li$_y$CrO$_{2+x}$/LiBO$_2$/WO$_3$/ITO	–	9–74	30	5×10^3	[21]
G/ITO/WO$_3$/LiAlF$_4$/V$_2$O$_5$/ITO	− 2/+ 1	11–50	90	–	[22]
G/ITO/WO$_3$/LiNbO$_3$/NiO/ITO	− 1.5/+ 1.5	8–72	2	2×10^3	[23]
G/ITO/WO$_3$/Ta$_2$O$_5$/NiO$_x$/ITO	− 5/+ 5	17–73	–	–	[24]
P/ITO/NiO$_x$/LiTaO$_3$/WO$_3$/ITO	− 4/+ 4	7–72	55	–	[25]
G/ITO/V$_2$O$_5$/LiPON/Li$_x$WO$_3$/TCO	− 1.5/+ 1.5	12–48	30	500	[26]

t_{sw} stands for switching time, *G and P* represent glass and plastic substrates, respectively, and (−) refers to not available data

into the device since Ta$_2$O$_5$ does not contain any H$^+$ or Li$^+$ ions. Recently, lithium phosphorus oxynitride (LiPON) solid electrolyte has attracted much interest because of its favorable electrochemical properties for thin film batteries and electrochromic devices [26–28]. However, this kind of lithium contained compound (e.g., LiNbO$_3$, LiTaO$_3$, LiAlF$_4$, LiBO$_2$) is normally not electrically conductive. The deposition techniques, such as radio frequency sputtering, thermal vacuum evaporation, and pulsed laser deposition, are not compatible with industrial large-scale manufacturing. And the deposition rate is also a big concern for commercial production.

Another major issue for inorganic electrolyte is the inherent leakage current. In fact, as the electrolyte is a very thin film, the five-layer designed monolithic solid state ECDs typically suffer from electronic leakage current and electronic breakdown [29, 30]. The leakage current may arise from pin holes or structural imperfections in the films. The device performance could be compromised including a lowered dynamic range, inhomogeneous coloration, rapid self-bleaching under open circuit, and slower switching speed. Therefore, it is necessary to add an electron blocking layer in the device. Recently, Bogati et al. [31] have investigated sputtered Si$_3$N$_4$ and SiO$_2$ as electron barrier between a redox electrolyte and the WO$_3$ film. They reported that the leakage current was significantly reduced with 80 nm of Si$_3$N$_4$ thin film in their system.

In the present work, a lithium magnesium nitride (Li$_x$Mg$_y$N) thin film was deposited by pulsed DC reactive sputtering as a Li$^+$ ion conducting layer. Si$_3$N$_4$ was applied as an electron blocking layer between the Li$_x$Mg$_y$N layer and the NiO layer. A monolithic solid state ECD was deposited by a series of room temperature DC sputtering processes on a single glass substrate. The multilayer structure can be described as Glass/ITO/NiO/Si$_3$N$_4$/Li$_x$Mg$_y$N/WO$_3$/ITO. The electro-optical properties of the ECD were investigated in detail.

Experimental details

Deposition of Li$_x$Mg$_y$N thin films

The Li$_x$Mg$_y$N thin films were deposited by pulsed DC reactive magnetron sputtering. The substrates were glass, silicon wafer, or silica glass. The target was a commercially available LiMg alloy (Li 20 wt%, Mg 80 wt%) plate of 10 cm in diameter and 6 mm in thickness. The target-substrate distance was 15 cm. Prior to the deposition, the substrates were ultrasonically cleaned in acetone, ethanol, and deionized water successively. The coating system was evacuated to a base pressure lower than 1×10^{-3} Pa by a turbo molecular pump combined with a rotary pump. LiMg alloy target was pre-sputtered in an argon atmosphere for 10 min in order to remove the surface contaminations. The flow rates of Ar (99.99%) and N$_2$ (99.99%) were controlled individually by mass flow controllers. During deposition, the flow rates of Ar and N$_2$ were 90 and 10 sccm, respectively. The total sputtering pressure was maintained at 0.8 Pa. The pulsed DC power was 180 W with a pulsing frequency of 40 kHz. The duty factor was 80% with a 20-μs sputter time and a 5-μs reverse time. Film uniformity was guaranteed by substrate rotation during the sputtering. The rotation speed was 5 rpm.

Fabrication of the electrochromic device

The ECD was performed in a multi-target magnetron sputtering system. All the targets used were 10 cm in diameter and 6 mm thick. The target-substrate distance was fixed at 15 cm. The sample holder was rotated (at 5 rpm) without intentional heating during the whole sputtering processes. ITO-coated glass having a sheet resistance of 30 Ω Sq^{-1} and an average transmittance of 85% in the visible region was used as the substrate. The layer stack can be described as Glass/ITO/NiO/Si_3N_4/Li_xMg_yN/WO_3/ITO. The performance of each individual layer was optimized prior to the fabrication of the ECD. Detailed sputtering parameters are listed in Table 2. The active size of the ECD was 5 × 5 cm^2.

Characterization

The structural properties were determined by X-ray diffraction (XRD) using a Rigaku D/MAX-2500/PC diffractometer with a Cu Kα source. The step size was 0.02°. The grazing incidence angle was 3° in parallel beam geometry with a 2θ between 10 and 90°. The cross-sectional images were acquired by scanning electron microscopy (SEM) using a XL30 S-FEG from FEI, equipped with energy dispersive X-ray spectroscopy (EDX). The film thicknesses of each layer were determined by both SEM cross-sectional observation and surface profilometry using a Dektak instrument. X-ray photoelectron spectroscopy (XPS) measurements were carried out in a VG Scientific ESCALab Mark II photoelectron spectrometer. Spectra were acquired using a monochromatic Al anode. Peak shifts due to charging were normalized by fixing the peak of adventitious carbon to 284.6 eV.

AC impedance measurements for the ionic conductivity of Li_xMg_yN thin films were conducted at room temperature (25 °C). An a.c. voltage with 100 mV amplitude within the frequency range from 1 Hz to 1 MHz was applied on the Glass/SS/Li_xMg_yN/SS sandwich configuration. The active size of the electrode was 1 mm^2. The ECDs were electrically characterized based on step chronoamperometry (CA) and cyclic voltammetry (CV). The electrical data were recorded with a CHI600E electrochemical workstation. The potential window was −4 V (coloration) and +2.5 V (bleaching) for both CA and CV measurements. The duration was 30 s for coloring step and 30 s for bleaching step in CA cycles. CV cycles were performed at a scan rate of 100 mV s^{-1}. Both CA and CV were measured for 1000 cycles, respectively. The optical transmittance data (at 600 nm) were acquired in situ during the electrochemical cycling of the ECD by using a Hitachi U-3010 UV-Vis spectrophotometer. The transmittance spectra of the device at its original, colored, and bleached states were measured over a wavelength of 300–800 nm.

Results and discussion

Figure 1 shows the XRD pattern of the Li_xMg_yN thin film prepared on a glass substrate. The big hump around 22° can be attributed to the glass substrate. The absence of diffraction peaks indicates that the as-deposited Li_xMg_yN thin film was amorphous.

XPS measurement was carried out to investigate the surface electronic state and chemical composition of the as-deposited Li_xMg_yN thin film. Figure 2a–c shows the XPS high-resolution spectra. A strong O 1s peak is observed, suggesting that the surface of the Li_xMg_yN film was oxidized. The binding energies of Li 1s (55.1 eV), C 1s (289.8 eV), and O 1s (531.5 eV) are in good accordance with Li_2CO_3. The binding energy of Mg 2p (49.4 eV) is accordance with $Mg(OH)_2$. The area of Li 1s region is much larger than Mg 2p region (see Fig. 2a). As the atomic sensitive factor of Mg 2p is much higher than Li 1s, it is implicated that the concentration of Li was much higher than Mg in the surface of the film. However, N 1s peak was not detected in the XPS measurement. In fact, moisture in the atmosphere can cause the degradation of Li_3N due to its reaction with H_2O to LiOH and NH_3, followed by further reaction with CO_2 to Li_2CO_3 at room temperature [32]. Mg_3N_2 can also react with H_2O to $Mg(OH)_2$ and NH_3. Therefore, the as-prepared Li_xMg_yN thin film was highly sensitive to atmosphere. Sun et al. [33] and Zhang et al. [34] have reported similar results of XPS spectra for Li_3N. They reported that the surface of Li_3N consisted of Li_3N, Li_2CO_3, and LiOH. Fig. 2d shows the EDX spectrum of the Li_xMg_yN thin film deposited on silicon wafer substrate. The N peak is observed in the spectrum. Based on the above discussion, the surface of the film was comprised of mainly Li_2CO_3, a small amount of $Mg(OH)_2$, and probable LiOH. The exact film composition was not available in this study. Li_3N is known as a fast lithium ion conductor [35]. Lapp et al. [36] have investigated the ionic conductivities of pure and doped Li_3N. They supposed that the incorporation of Mg^{2+} substitutional ions in the Li_3N lattice might be expected to create Li^+ vacancies for charge compensation, thereby, increasing the number of mobile Li^+ ions. But the actual conductivities (1.0×10^{-4} S cm^{-1}) they obtained were not increased. Figure 3 shows a Nyquist impedance spectrum of a 300-nm thick Li_xMg_yN film. The ionic conductivity σ was determined by using the equation of $\sigma = d$ ($R \times A$), where d is the thickness of the electrolyte, R is the resistance of the electrolyte, and A is the area of the electrode. The calculated ionic conductivity of the Li_xMg_yN film was 3.3×10^{-9} S cm^{-1}. This value is much lower than the value reported by Lapp et al. (Mg doped Li_3N crystal, bulk, 1.0×10^{-4} S cm^{-1}). The amorphous structure of the Li_xMg_yN film might compromise the mobility of Li^+ ions, and it should be mentioned that the residual oxygen in the chamber was probably incorporated into the Li_xMg_yN film during the sputtering process. This value is also lower than the ionic conductivity of LiPON thin films studied by Oukassi et al. (2.7×10^{-6} S cm^{-1}) [26] and Su et al. (4.9×10^{-6} S cm^{-1}) [27].

Table 2 Deposition conditions for each layer of the electrochromic device

Film	Target	Power[a] (W)	Pressure (Pa)	Ar/O$_2$/N$_2$ (sccm)	Thickness (nm)
NiO	Ni	DC, 230	3	94/6/0	300
Si$_3$N$_4$	SiAl[b]	p-DC, 235	0.5	40/0/10	150
Li$_x$Mg$_y$N	LiMg[c]	p-DC, 180	0.8	100/0/10	300
WO$_3$	W	DC, 300	2.2	30/10/0	300
ITO	ITO	DC, 210	0.3	98/2/0	300

[a] DC and p-DC refer to direct current and pulsed direct current power sources, respectively

[b] Composition of SiAl alloy target is 90 wt% Si, 10 wt% Al

[c] Composition of LiMg alloy target is 20 wt% Li, 80 wt% Mg

The ECD fabricated in this research comprised WO$_3$ and NiO as the electrochromic active layers, Li$_x$Mg$_y$N as the electrolyte layer, and Si$_3$N$_4$ as an electron blocking layer. The cross-sectional SEM image in Fig. 4 displays the layer stacks of the ECD. The ECD without the Si$_3$N$_4$ layer, however, did not show stable and reversible coloration/bleaching in our study. The cyclic voltammogram (CV) showed mainly a straight line which indicated no capacitance characteristics. This is most likely caused by the poor dielectric property of the Li$_x$Mg$_y$N layer. The required voltage is shorted out, and the movements of lithium ions are suppressed due to the electronic currents which leak or pass through the ion conducting layer. According to Bogati et al. [31], we have applied Si$_3$N$_4$ as a buffer layer between the Li$_x$Mg$_y$N layer and the NiO layer. In our case, the optimal thickness of Si$_3$N$_4$ was around 150 nm. As indicated in Fig. 5a, the transportation of Li$^+$ ions in Si$_3$N$_4$ was fast and only a little decrease of charge capacity was observed. Fig. 5b shows the CV curves of NiO and Si$_3$N$_4$-covered NiO in Mg^{2+}-containing electrolyte. The big reduction of current density implies that the Mg^{2+} ion intercalation into NiO film can be partially blocked by Si$_3$N$_4$ layer. This provides another benefit for the device that the unwanted effect of possible Mg^{2+} ion intercalation into NiO layer could be inhibited by Si$_3$N$_4$ layer.

Transmittance spectra over a wavelength of 300–800 nm of the ECD in original, bleached, and colored states are shown in Fig. 6a. The cyclic voltages were −4 V for coloration and

Fig. 1 XRD pattern of the Li$_x$Mg$_y$N thin film deposited on glass

2.5 V for bleaching, respectively. The optical modulation in the visible region is around 40% in average. The optical absorption at around 400 nm and residual color in the bleached device arise from NiO layer and top ITO layer, not from Li$_x$Mg$_y$N layer which is highly transparent in the visible region as shown in Fig. 6d. It should be mentioned that the electric resistance of the top ITO layer was high (150 Ω Sq^{-1}). The device required a high potential window to obtain a large optical modulation which can be attributed to the large resistance of the ITO electrode and also the comparatively low ionic conductivity of the Li$_x$Mg$_y$N ion conductor. Figure 6b, c presents the bleached and colored states of the ECD. It is demonstrated that the coloration is homogeneous, and the color is neutral.

To study the dynamics of the switching process and test the electrochemical stability of the device, both step chronoamperometric cycles (CA) and cyclic voltammetries (CV) were carried out for 1000 cycles, respectively. The optical transmittance at 600 nm of the device was measured in real-time. The transmittance data of the ECD during 1000 CA cycles are shown in Fig. 7a. Except for the first few cycles, the bleached transmittance is maintained at a constant value of nearly 70%. The lowered bleached transmittance at the beginning is caused by the initial cycling of the NiO layer, which usually exhibits increased bleached transmittance upon multiple cycles of deintercalation/intercalation of lithium ions and electrons. The colored transmittance is first decreased to 30% in the first 200 cycles and then gradually increased to 45%. Figure 7b, c shows the CA curves of the device and the corresponding optical modulation (ΔT). It is evident that the device has an activation period and degradation period. The electrical activation and optical activation take place in the first 50 cycles. However, the electrical degradation begins immediately after the electrical activation, while the optical degradation begins after 200 cycles. The optical steady period sustains 150 CA cycles before apparent degradation. It is observed in Fig. 7c that the bleaching peak current drops much faster than coloration current after 50th CA cycle. The bleached transmittance also decreases after 5000 s as shown in Fig. 7a. We believed that this phenomenon is mainly associated with the degradation of NiO layer. According to Passerini et al. [37–39], electrochromism of nickel oxide in
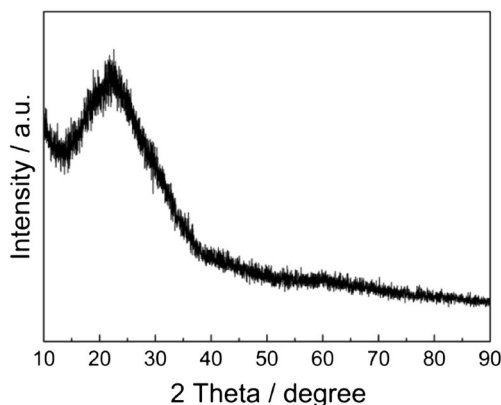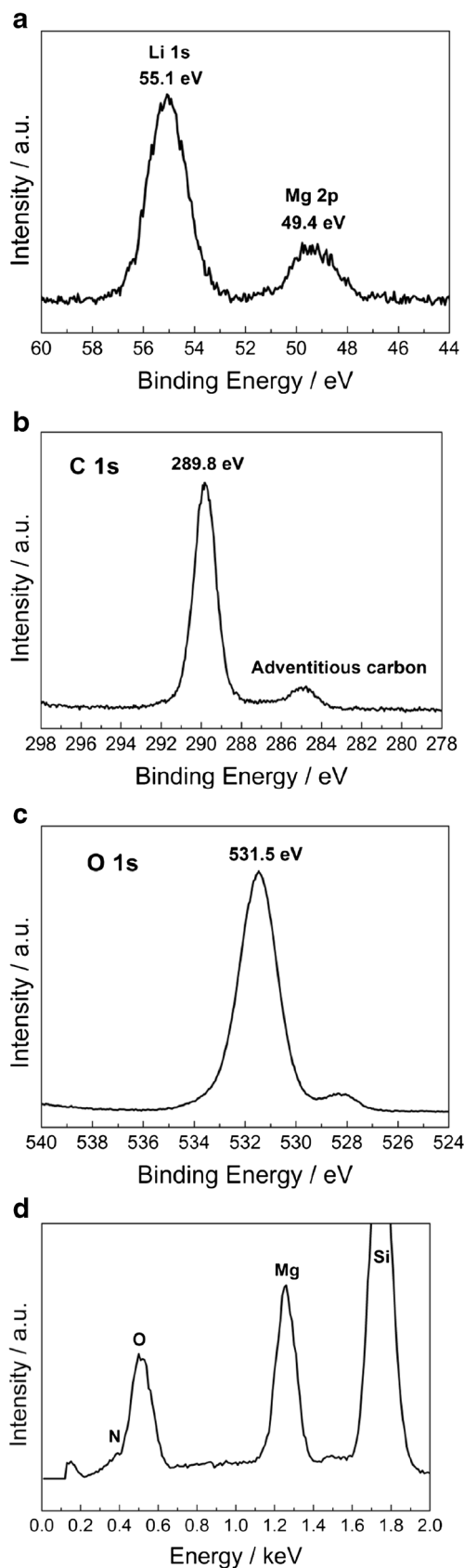
Li containing electrolyte can be interpreted by a two-step process with an initial activation by

$$NiO + yLi^+ + ye^- \rightarrow Li_yNiO \quad (1)$$

followed by a reversible reaction between bleached Li$_y$NiO and colored Li$_{(y-z)}$NiO according to

$$Li_yNiO \leftrightarrow Li_{(y-z)}NiO + zLi^+ + ze^- \quad (2)$$
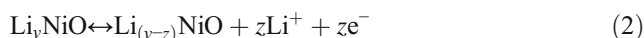
Wen et al. [40] reported that degradation of nickel oxide thin film in LiClO$_4$-PC was much faster than in KOH. The variation of bleached transmittance during the initial cycles can be explained by the activation and poor cycling durability of NiO film in Li based system.

As mentioned above, the inherent leakage current is a major concern to monolithic inorganic ECDs. Leakage current is defined as the steady state current when the rate of color changing becomes zero [30]. It is noteworthy that the leakage current in the ECD at colored state is decreased after 1000 CA cycles as indicated in Fig. 7b. Figure 8 illustrates the test results of open circuit memory effect of the ECD after 20 and 1000 CA cycles. The decreased leakage current after 1000 CA cycles leads to a better memory effect of the ECD. However, the coloration time is increased to reach the same colored level. Moreover, the CA current density during darkening of the device after 1000 cycles shows an anomalous slope which may be associated with a complex formatting process in the NiO layer. The origin of this needs further study.

Figure 9a shows the cyclic voltammograms of the ECD for 1000 cycles and Fig. 9b shows the corresponding evolution of the transmittance at 600 nm. Compared with CA cycles, the
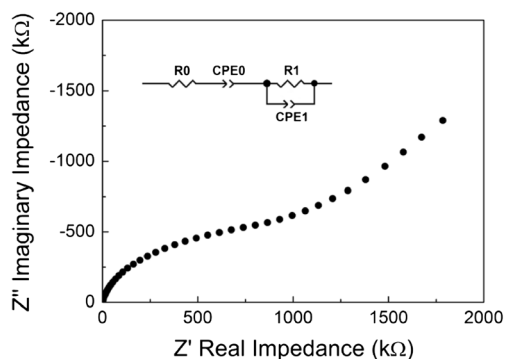

Fig. 3 Nyquist impedance plots of 300 nm thick Li$_x$Mg$_y$N thin film with an active electrode area of 1 mm^2 at 25 °C. The equivalent circuit model is also shown
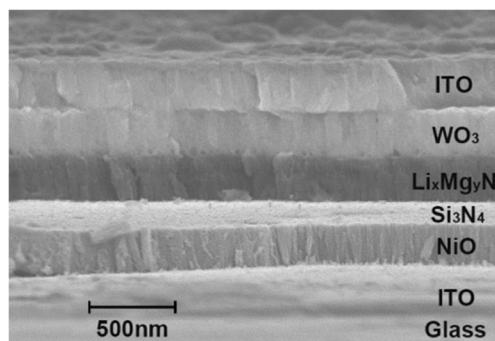
Fig. 4 Cross-sectional SEM micrograph of the complete electrochromic device

CV cycles exhibit both good electrical and optical stability. The degradation of chronoamperometric cycles is much faster than cyclic voltammetries. This is associated with high current densities involved during the switching process. As discussed by Nagai et al. [16], defects in layer formation introduce hot spots which can act as degradation seed for the surrounding area. The degradation will be faster depending on the characteristic resistance of this hot spot. As expected, the CV cycles also show activation process which is though not as distinct as CA cycles. It takes 200 cycles to activate for CV cycles which is much slower than CA cycles. This also can attribute to the high current densities of the CA cycles.
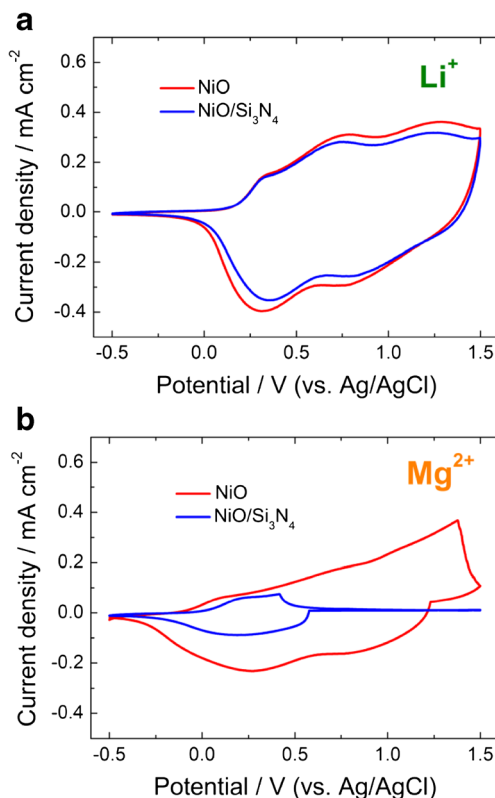
Fig. 5 Cyclic voltammograms of NiO and Si_3N_4-covered NiO in (**a**) 1 M $LiClO_4$-PC electrolyte and (**b**) 1 M $Mg(ClO_4)_2$-PC electrolyte, at a scan rate of 20 mV s^{-1}
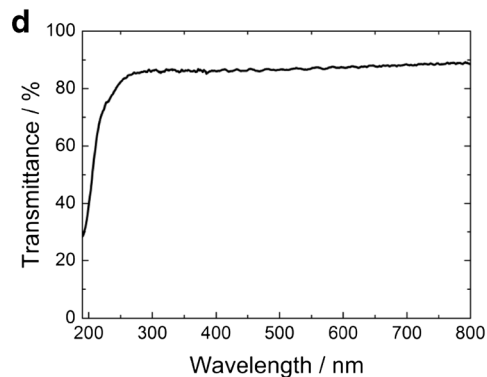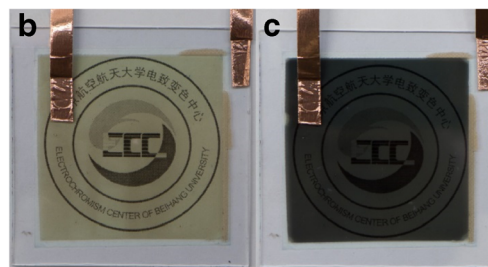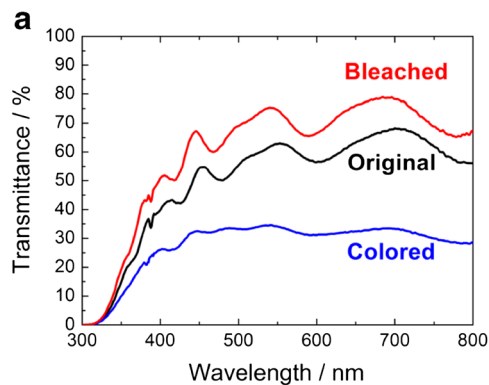

Fig. 6 **a** Optical transmittance spectra of the electrochromic device in original, bleached, and colored states. **b** Photograph of the bleached device. **c** Photograph of the colored device. The active size of the device was 5×5 cm^2. **d** Transmittance spectra of 300 nm thick Li_xMg_yN thin film deposited on a silica glass substrate

Coloration efficiency (CE) is defined as the change of optical density (ΔOD) at a certain wavelength per unit of inserted (or extracted) charge density (ΔQ). The formula is defined as follows:

$$CE = \frac{\Delta OD(\lambda)}{\Delta Q} \tag{3}$$

$$\Delta OD(\lambda) = \log\left(\frac{T_b}{T_c}\right) \tag{4}$$

where CE denotes coloration efficiency, T_b and T_c refer to the optical transmittance of the film in bleached and colored states, respectively. It is desirable for most electrochromic devices that the CE should be as large as possible. The calculated values of transferred charge and coloration efficiency are
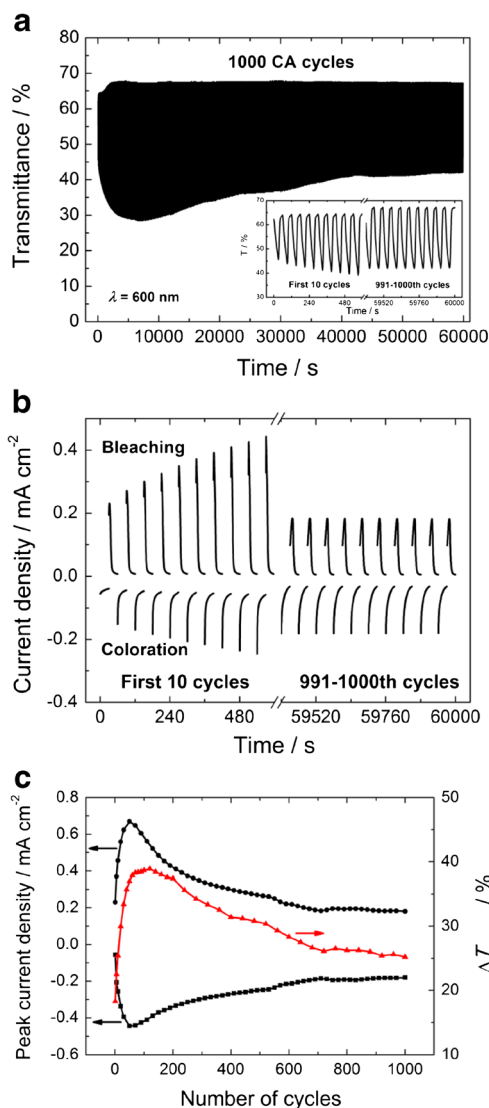
Fig. 7 **a** Evolution of transmittance at 600 nm of the ECD during the 1000 CA cycles. The inset displays the details of the first and last 10 cycles. **b** Step chronoamperometric curves of the device. **c** Evolution of peak current density and the corresponding recorded optical modulation at 600 nm in real-time during the 1000 CA cycles
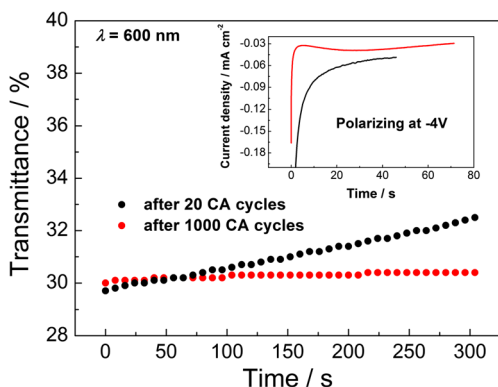

Fig. 9 **a** Cyclic voltammograms of the ECD for 1000 cycles. The arrows represent the sweeping direction. **b** In situ measurement of the transmittance at 600 nm during the 1000 CV cycles. **c** The calculated transferred charge during coloration/bleaching and coloration efficiency of the ECD for 1000 CV cycles

Fig. 8 Memory test of the ECD showing the self-bleaching transmittance at 600 nm under open circuit. The inset shows the chronoamperometric current of coloration process before the memory test
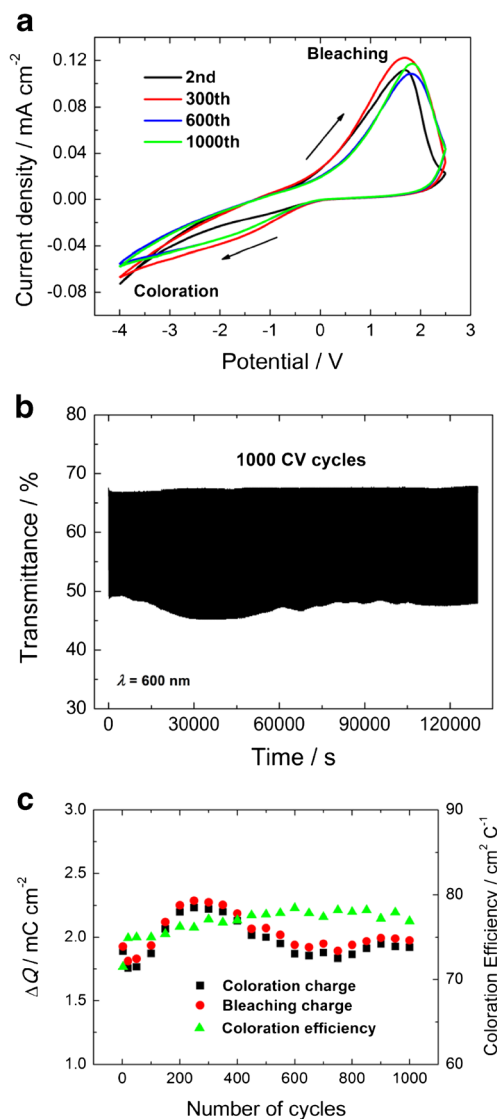
plotted in Fig. 9c. The charge density increases in the first 200 CV cycles and then slightly decreases to a stable state, while the coloration efficiency increases during the initial sweeps and tends towards stability upon subsequent cycles. The amounts of transferred charge during coloration and bleaching are basically equal, which demonstrates reversible electrochemical reactions. The value of coloration efficiency is approximately 77 $cm^2 C^{-1}$, which is comparable to the reported values adopting complementary electrochromic layers [14, 41, 42]. A high coloration efficiency was achieved owing to the electrochromic effects of both WO_3 and NiO layers. The value of charge capacity is only around 2 $mC cm^{-2}$ which limits the electrochromic performance of the device. This demonstrates that the as-deposited Li_xMg_yN layer had a limited Li ionic

conductivity. As discussed above, its amorphous structure and incorporation of Mg^{2+} ions into Li_3N network might compromise the mobility of Li^+ ions. Moreover, it is highly likely that the residual oxygen was incorporated into the Li_xMg_yN layer during sputtering.

It is interesting that the cycling process of the ECD involved an initial activation stage. This is mainly related to the Li_xMg_yN layer and Si_3N_4 layer. With the increased cycles, more diffusion pathways were opened up for Li^+ ions. It also should be mentioned that the amounts of charge insertion (extraction) in WO_3 layer and extraction (insertion) from NiO layer were unbalanced during the first few cycles. There are several possible reasons that may contribute to the degradation of the electro-optical characteristics of the device, and among these are (1) atmospheric interaction (moisture or oxygen), (2) degradation of the Li_xMg_yN layer, and (3) Li^+ ions trapping in WO_3 or NiO during the cyclic process.

Conclusions

Li_xMg_yN thin films were prepared by pulsed DC reactive magnetron sputtering from a commercially available LiMg alloy target. XRD indicated that the films were amorphous. XPS analysis revealed a surface composition of predominant Li_2CO_3, $Mg(OH)_2$, and probable LiOH, and the N peak was observed in EDX spectrum. The calculated ionic conductivity of the Li_xMg_yN film was 3.3×10^{-9} S cm^{-1}. The integration of Li_xMg_yN film into the electrochromic device was successful when a 150 nm thick Si_3N_4 layer was added between Li_xMg_yN layer and NiO layer. The leakage current in the ECD was significantly reduced by Si_3N_4; moreover, the possible Mg^{2+} ion intercalation into NiO layer could be suppressed. The ECD fabricated under the optimized conditions showed an optical modulation of around 40% in the visible region. Chronoamperometric cycles demonstrated evident activation and degradation of the electro-optical properties of the ECD. While the voltammetric cycles were comparatively stable, this can be attributed to the high current densities during the CA cycles, which accelerated the activation and degradation processes of the device. The open circuit memory effect was improved with the increased CA cycles. Some unknown changes may take place in Li_xMg_yN layer or Si_3N_4 layer which needs further investigation. The charge density of the ECD was 2 mC cm^{-2}, and the coloration efficiency was around 77 cm^2 C^{-1} at 600 nm. Further work is required to improve the electrochromic performance and cycling durability of the device.

References

1. Granqvist CG (1995) Handbook of inorganic electrochromic materials. Elsevier, Amsterdam
2. Monk PMS, Mortimer RJ, Rosseinsky DR (2007) Electrochromism and electrochromic devices. Cambridge University Press, Cambridge
3. Lampert CM (1984) Electrochromic materials and devices for energy efficient windows. Sol Energy Mater 11:1–27
4. Baetens R, Jelle BP, Gustavsen A (2010) Properties, requirements and possibilities of smart windows for dynamic daylight and solar energy control in buildings: a state-of-the-art review. Sol Energy Mater Sol Cells 94:87–105
5. Rosseinsky DR, Mortimer RJ (2001) Electrochromic systems and the prospects for devices. Adv Mater 13:783–793
6. Coleman JP, Lynch AT, Madhukar P, Wagenknecht JH (1999) Printed, flexible electrochromic displays using interdigitated electrodes. Sol Energy Mater Sol Cells 56:395–418
7. Niwa T, Takai O (2010) All-solid-state reflectance-type electrochromic devices using iridium tin oxide film as counter electrode. Thin Solid Films 518:5340–5344
8. Sauvet K, Sauques L, Rougier A (2009) IR electrochromic WO_3 thin films: from optimization to devices. Sol Energy Mater Sol Cells 93:2045–2049
9. Demiryont H, Moorehead D (2009) Electrochromic emissivity modulator for spacecraft thermal management. Sol Energy Mater Sol Cells 93:2075–2078
10. Niklasson GA, Granqvist CG (2007) Electrochromics for smart windows: thin films of tungsten oxide and nickel oxide, and devices based on these. J Mater Chem 17:127–156
11. Deb SK (2008) Opportunities and challenges in science and technology of WO_3 for electrochromic and related applications. Sol Energy Mater Sol Cells 92:245–258
12. Moulki H, Park DH, Min BK, Kwon H, Hwang SJ, Choy JH, Toupance T, Campet G, Rougier A (2012) Improved electrochromic performances of NiO based thin films by lithium addition: from single layers to devices. Electrochim Acta 74:46–49
13. Xia XH, Tu JP, Zhang J, Wang XL, Zhang WK, Huang H (2008) Morphology effect on the electrochromic and electrochemical performances of NiO thin films. Electrochim Acta 53:5721–5724
14. Subrahmanyam A, Kumar CS, Karuppasamy KM (2007) A note on fast protonic solid state electrochromic device: $NiO_x/Ta_2O_5/WO_{3-x}$. Sol Energy Mater Sol Cells 91:62–66
15. Mathew JGH, Sapers SP, Cumbo MJ, O'Brien NA, Sargent RB, Raksha VP, Lahaderne RB, Hichwa BP (1997) Large area electrochromics for architectural applications. J Non-Cryst Solids 218:342–346
16. Nagai J, McMeeking GD, Saitoh Y (1999) Durability of electrochromic glazing. Sol Energy Mater Sol Cells 56:309–319
17. Larsson AL, Niklasson GA (2004) Optical properties of electrochromic all-solid-state devices. Sol Energy Mater Sol Cells 84:351–360
18. Patel KJ, Desai MS, Panchal CJ (2015) Studies of ZrO_2 electrolyte thin-film thickness on the all-solid thin-film electrochromic devices. J Solid State Electrochem 19:275–279
19. Goldner RB, Arntz FO, Berera G, Haas TE, Wei G, Wong KK, Yu PC (1992) A monolithic thin-film electrochromic window. Solid State Ionics 53-56:617–627
20. Ashrit PV, Girouard FE, Truong VV (1996) Fabrication and testing of an all-solid state system for smart window application. Solid State Ionics 89:65–73
21. Cogan SF, Rauh RD, Klein JD, Nguyen NM, Jones RB, Plante TD (1997) Variable transmittance coatings using electrochromic lithium chromate and amorphous WO_3 thin films. J Electrochem Soc 144:956–960

22. Daneo A, Macrelli G, Polato P, Poli E (1999) Photometric characterization of an all solid state inorganic electrochromic large area device. Sol Energy Mater Sol Cells 56:237–248

23. Zhang X, Zhang H, Li Q, Luo H (2000) An all-solid-state inorganic electrochromic display of WO_3 and NiO films with $LiNbO_3$ ion conductor. IEEE Electr Device L 21:215–217

24. Wang SC, Liu KY, Huang JL (2011) Tantalum oxide film prepared by reactive magnetron sputtering deposition for all-solid-state electrochromic device. Thin Solid Films 520:1454–1459

25. Liu Q, Dong G, Xiao Y, Gao F, Wang M, Wang Q, Wang S, Zuo H, Diao X (2015) An all-thin-film inorganic electrochromic device monolithically fabricated on flexible PET/ITO substrate by magnetron sputtering. Mater Lett 142:232–234

26. Oukassi S, Giroud-Garampon C, Dubarry C, Ducros C, Salot R (2016) All inorganic thin film electrochromic device using LiPON as the ion conductor. Sol Energy Mater Sol Cells 145:2–7

27. Su Y, Falgenhauer J, Polity A, Leichtweiß T, Kronenberger A, Obel J, Zhou S, Schlettwein D, Janek J, Meyer BK (2015) LiPON thin films with high nitrogen content for application in lithium batteries and electrochromic devices prepared by RF magnetron sputtering. Solid State Ionics 282:63–69

28. Knauth P (2009) Inorganic solid Li ion conductors: an overview. Solid State Ionics 180:911–916

29. Granqvist CG (2012) Oxide electrochromics: an introduction to devices and materials. Sol Energy Mater Sol Cells 99:3

30. O'Brien NA, Gordon J, Mathew H, Hichwa BP (1999) Electrochromic coatings—applications and manufacturing issues. Thin Solid Films 345:312–318

31. Bogati S, Georg A, Graf W (2017) Sputtered Si_3N_4 and SiO_2 electron barrier layer between a redox electrolyte and the WO_3 film in electrochromic devices. Sol Energy Mater Sol Cells 159:395–404

32. Zhang J, Hu Y (2015) Higher chemical stability of α-Li_3N than β-Li_3N in atmosphere. Top Catal 58:386

33. Sun Y, Li Y, Sun J, Li Y, Pei A, Cui Y (2017) Stabilized Li_3N for efficient battery cathode prelithiation. Energy Storage Mater 6:119–124

34. Zhang YJ, Wang W, Tang H, Bai WQ, Ge X, Wang XL, Gu CD, Tu JP (2015) An ex-situ nitridation route to synthesize Li_3N-modified Li anodes for lithium secondary batteries. J Power Sources 277: 308–310

35. Tapia-Ruiz N, Segalés M, Gregory DH (2013) The chemistry of ternary and higher lithium nitrides. Coord Chem Rev 257:1987

36. Lapp T, Skaarup S, Hooper A (1983) Ionic conductivity of pure and doped Li_3N. Solid State Ionics 11:98

37. Passerini S, Scrosati B, Gorenstein A (1990) The intercalation of lithium in nickel oxide and its electrochromic properties. J Electrochem Soc 137:3297

38. Passerini S, Scarminio J, Scrosati B, Zane D, Decker F (1993) Thin metal oxide films on transparent substrates for Li-insertion devices. J Appl Electrochem 23:1187

39. Passerini S, Scrosati B (1992) Electrochromism of thin-film nickel oxide electrodes. Solid State Ionics 53–56:520

40. Wen RT, Niklasson GA, Granqvist CG (2014) Electrochromic nickel oxide films and their compatibility with potassium hydroxide and lithium perchlorate in propylene carbonate: optical, electrochemical and stress-related properties. Thin Solid Films 565:133

41. Zhang J, Tu JP, Xia XH, Qiao Y, Lu Y (2009) An all-solid-state electrochromic device based on NiO/WO_3 complementary structure and solid hybrid polyelectrolyte. Sol Energy Mater Sol Cells 93: 1842

42. Ahn KS, Nah YC, Sung YE, Cho KY, Shin SS, Park JK (2002) All-solid-state electrochromic device composed of WO_3 and $Ni(OH)_2$ with a Ta_2O_5 protective layer. Appl Phys Lett 81:3930–3932